Laser Innovations for Research and Applications

journal homepage: https://lira.journals.ekb.eg/

ISSN: Print 3009-6359 / Online 3009-6472

A comprehensive review of nonlinear optical properties of ITO semiconductor material

Fatma Abdel-Samad[1], Alaa Mahmoud[1], Tarek Mohamed[1*]

[1]Laser Institute for Research and Applications (LIRA), Beni-Suef University, Beni-Suef 62511, Egypt

Abstract

Transparent conducting oxide (TCO) materials have unique electrical and optical features. One of many TCOs widely employed in practical optoelectronic devices is indium tin oxide (ITO). Many characterization techniques are used to study materials' nonlinear optical (NLO) properties. The simplest and most accurate technique among these is the Z-scan technique, which is widely used. This article introduces a comprehensive review of the optical nonlinearity of the interaction of a high-intensity laser source with an ITO semiconductor material as a promising material for NLO applications.

Keywords: Transparent conducting oxide; Nonlinear optical properties; Z-scan technique; ITO semiconductor; Nonlinear absorption; Nonlinear refraction.

***Corresponding author at: Laser Institute for Research and Applications LIRA, Beni-Suef University, Beni-Suef 62511, Egypt

E-mail addresses: tarek_mohamed1969@lira.bsu.edu.eg

1. Introduction

Nonlinear optics (NLO) is one of the branches of nonlinear physics. NLO materials have attracted the attention of many researchers, particularly with the development of ultrashort laser pulses (Masters & Boyd, 2009). NLO is the investigation of nonlinear phenomena in the interaction of a laser and a material (He & Liu, 1999). The study of a phenomenon that causes a change in a material's optical properties is called nonlinear optics. This change occurs when a medium is irradiated with a high-intensity laser source. A force is applied to all of the electrons in a medium by an external electromagnetic field (Boyd). Pump light is one of the two factors that cause a change in matter's macroscopic parameters, such as susceptibility, refractive index, absorption coefficient, and so on, or a change in matter's microscopic structure, resulting in "light-controlling matter" (Vasconcelos, 2022). The other is investigating changes in the signal light propagating parameters in the matter, such as frequency, power, phase, pulse width, group velocity, and so on (Diels & Rudolph, 2006). Although most nonlinear optical phenomena can only be observed with laser radiation, some were known long before the invention of the laser. Pockels' and Kerr's electro-optic effects are two prominent examples of such phenomena. In 1875, John Kerr reported an induced alteration in the refractive index of CS_2 proportional to the square of an applied electric field (the Kerr effect) (Kerr, 1875). In 1893, the Pockels effect was observed, similar to a linear electric field in quartz (New, 2011). Before lasers, the most intense power source available was lamps, which typically produced powers in the order of 100 W. However, because of their high divergence and broad emission spectrum, they are ineffective for probing weak nonlinear optical phenomena. By comparison, lasers are monochromatic and highly directional sources capable of producing intensities in excess of 106 W/cm_2, which is comparable to the range of the inter-atomic fields. The birth of experimental NLO phenomena began with the manufacture of the first laser in 1960 (Arun Kumar, 2013). The demonstration of the Second Harmonic Generation (SHG) of the fight by a ruby laser pulse in a quartz crystal by Franken and colleagues (Franken et al., 1961) in 1961 marked the beginning of nonlinear optics as a new separate subfield of scientific endeavor, as shown in Fig.1. Kaiser and Garret studied the same photon energies or two-photon absorption (2PA)

induced fluorescence in a CaF_2: Eu^{2+} crystal and published their experimental results (Kaiser & Garrett, 1961). 2PA was expected by M. Göppert Mayer in 1931 (W. Wang et al., 2010) and was confirmed by Kaiser and Garret's experiments. These works are widely regarded as the origins of nonlinear optics. NLO materials play a crucial role in the development of all-optical and electro-optical systems with applications in optical communications, light-driven chemical reactions, and optical computing (Correa et al., 2011; Kowalevicz et al., 2005; Li et al., 2002; Mançois et al., 2009). High NLO properties have been found in organic and inorganic molecules (Gabler et al., 1997), polymers (Zaid et al., 2015), and semiconductors (Grehn et al., 2013; Santos et al., 2017).

Many techniques are used to investigate the NLO properties of materials (Adair et al., 1987; Miguez et al., 2014; Moran et al., 1975; Owyoung, 1973; Williams et al., 1984), but they are relatively complex experimental tools, inaccurate, and require detailed wave propagation analysis (Soileau et al., 1983). Sheik-Bahae developed the single-beam Z-scan technique, which is considered the simplest technique for determining the NLO properties of new materials (Lee et al., 1994; Sheik-Bahae et al., 1989b). These NLO properties involve the nonlinear absorption (NLA) coefficient and the nonlinear refractive (NLR) index of the material (Gu & Wang, 2011; Kalanoor et al., 2016). The NLA coefficient (β) and the NLR index (n_2) were experimentally studied using both open aperture (OA) and close aperture (CA) Z-scan techniques (Shehata & Mohamed, 2019; Shehata et al., 2020). NLA is the change in a material's transmittance as a function of incident intensity or excitation wavelength. Because of its several applications in science and technology, including Q-switching and mode-locking, nonlinear spectroscopy, up-conversion lasing, fluorescence imaging, and optical limiting, NLA has attracted a lot of attention (Q. Guo et al., 2016; Hales et al., 2010; Liu et al., 2017; Min et al., 2011; Mukhopadhyay et al., 2012; Tian et al., 2018). Two-photon absorption (2PA), a type of NLA effect, involves the simultaneous absorption of two photons from the low energy state, which is generally the ground state, to the high energy state (Reyna et al., 2018). Characterizing the 2PA properties of a nonlinear material is critical for any practical applications. Two-photon fluorescence imaging (Denk et al., 1990b), two-photon microfabrication (Maruo et al., 1997b), and three-dimensional optical data

storage (J. H. Strickler & W. W. J. O. l. Webb, 1991) are all applications that use 2PA processes. In addition, optical limiters used in sensor protection require two-photon absorbers (Van Stryland et al., 1988b). Sheik-Bahai et al. (Lee et al., 1994) pioneered the OA Z-scan technique, which is well known for being a highly efficient technique for studying the NLA properties of different materials. NLR is the process by which light changes a material's NLR properties. The n_2 is a crucial parameter in the development of ultrafast all-optical switching devices and modern optical communication systems (Weiner, 2011).

Transparent conducting oxides (TCO) materials are one of these materials. Because of their broad bandgap of 3 to 4.2 eV) Hamberg & Granqvist, 1986(, TCO thin films have unique electrical and optical features, including high conductivity, high free carrier density, and strong optical transmission in the visible region (Asobe et al., 1992; H. Wang et al., 2010). TCO thin films are used for many applications, such as plasma displays (Wager, 2003), solar cells (Lien, 2010), and light-emitting diodes (Afre et al., 2018; Betz, Olsson, Marthy, Escolá, Atamny, et al., 2006). TCO materials exhibit strong nonlinear properties under both inter-band and intra-band excitations (Clerici et al., 2017). In the case of energy-absorbing nonlinear processes, the TCO materials can be categorized into two types: saturable absorption (SA) (increased transmittance) or reverse saturable absorption (RSA) (decreased transmittance). The electrons in the ground state absorb incident energy and transition to the excited state, resulting in the SA behaviour (Sridharan et al., 2015), where decreasing absorption with increasing incident light intensity results in saturation of the excited state or bleaching of the ground state (Ashour et al., 2022). In contrast, the RSA behavior is caused by excited-state absorption (ESA), multiphoton absorption (MPA), and free-carrier absorption (FCA) (Elim et al., 2006), in which absorption increases with increasing light intensity. The SA phenomenon is necessary for using TCO in mode-locking (Guo et al., 2019b) and passive Q-switching techniques to generate ultrashort pulse lasers (Guo et al., 2017). At the same time, the most crucial application of RSA is optical limiters for the protection of sensitive optical components, including human eyes from laser-induced damage (Liu et al., 2009). TCO thin films are made from a range of materials, including indium, tin, cadmium, and zinc oxides, as well as mixtures of these metals (Benoy et al.,

2009). Indium-doped tin oxide (ITO) films have received a lot of attention in comparison to other transparent conducting oxides (Park, Kim, Lee, Kim, Lee, et al., 2010). Because of the enormous number of oxygen vacancies (J. C. Fan & J. B. J. J. o. A. P. Goodenough, 1977; Giusti, 2011; Ma et al., 2015b; Nadaud et al., 1998b) and the substitution of Sn dopants in ITO thin films, they are usually n-type semiconductors (A. Eshaghi & A. J. O. Graeli, 2014; Wohlmuth & Adesida, 2005). The ITO thin film has the general chemical formula of $In_4Sn_3O_{12}$ and has low electrical resistivity, high optical transparency (over 80%) in the visible wavelength range with simultaneous high reflection in the IR, and good chemical stability (Coutts et al., 1990; Ma et al., 2021b). Because of these properties, ITO is widely used in many fields, including optics and electronics. Multiple uses of ITO range from photovoltaics to conductive displays, integrated photonics, solar cells, electroluminescent devices, charge-coupled devices, and also for NLO applications (Alam et al., 2016; Moran et al., 1975). Many fantastic NLO effects of ITO film have recently been exploited, including nonlinear absorption (P. Guo, R. D. Schaller, J. B. Ketterson, & R. P. J. N. P. Chang, 2016; Xiao et al., 2020b), Kerr nonlinearity (Khurgin et al., 2020b; Kinsey et al., 2015b; Moran et al., 1975), and four-wave mixing (Huh et al., 2008).

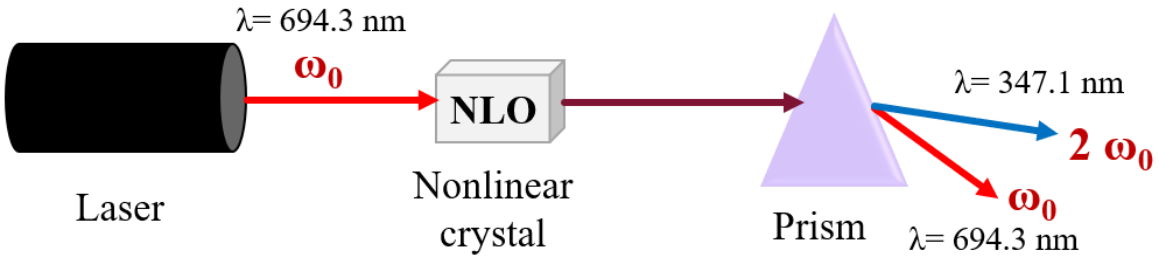

Fig. 1. A schematic diagram of the second harmonic generation experiment in quartz by Peter Franken's group at the University of Michigan in 1961.

2. Nonlinear optical responses in materials

The field that binds electrons to atoms is much higher than the radiation field of a light source. Electron deviations from equilibrium are minor. In an atom, the nucleus is surrounded by electron clouds, and the atom's net charge is zero due to their spherical shape. When an electric field is applied to an atom, the electrons move in the opposite direction of the field, transforming the cloud into an

ellipsoid. The electric field acting on the atom's positive and negative charges distorts the electron charge distribution. The electric dipole moment (μ) induced in the atom by the electric field is a primary measure of this distortion, μ= -ex Where e is the charge of an electron at the point denoted by the displacement vector x. When an electric field is applied to a medium, the electric dipole moment μ= αE, where is the polarizability of the individual atoms (Walden, 2017). When all of a material's electrons oscillate at the same time, the collective motion induces a macroscopic polarization, which is related to the dipole moment by P = Nμ = NαE, where N is the material's dipole concentration or electron density (Walden, 2017). Similarly, instead of using the microscopic quantity of polarizability, the macroscopic equivalent of susceptibility χ can be used, which is related to the polarizability by $\varepsilon_0 \chi = N\alpha$ where ε_0 is the permittivity of free space. Figure 2 depicts the linear relationship between induced polarization and applied electric field strength, as described in conventional (i.e., linear) optics by the relationship

$$P = \varepsilon_0 \chi E \quad (1)$$

The susceptibility is affected by incident field properties such as amplitude, wavelength, and polarization, as well as material properties such as concentration and orientation (Nagaraja et al., 2013). Maxwell's equation $E = E_0 - P/\varepsilon_0$ describes the total electric field inside the irradiated material as a result of the applied field and the induced polarization. Given that the polarization is dependent on the applied field, the total induced field can be rewritten as $E= (1+ \chi) E_0 = \varepsilon_r E_0$ where $\varepsilon_r = 1+ \chi$ is the material's relative permittivity.

In the case of high–intensity electromagnetic radiation, such as a laser beam irradiates a medium. As shown in Fig 2, the nonlinear behaviour of the polarization response is related to the applied electric field strength (Petkova et al., 2016; Shen, 1984). The polarization response of the medium can be expanded into a power series in E in the frequency domain to describe the nonlinear effects (Shen, 1984). Individual atoms' higher-order polarizability is incorporated into material susceptibility by including intensity-dependent terms (Sauter, 1996). Then χ can be expressed as

$$\chi = \chi^{(1)} + \chi^{(2)} E + \chi^{(3)} EE + \ldots \quad (2)$$

Where $\chi^{(1)}$ is the linear response of polarization expansion, $\chi^{(2)}$ is the second-order susceptibility, $\chi^{(3)}$ is the third-order susceptibility, and so on for higher orders. These higher-order susceptibilities induce polarization in the material and can be expressed as

$$P = \varepsilon_0 (\chi^{(1)} E + \chi^{(2)} EE + \chi^{(3)} EEE + \ldots) = P^{(1)} + P^{(2)} + P^{(3)} + \ldots \quad (3)$$

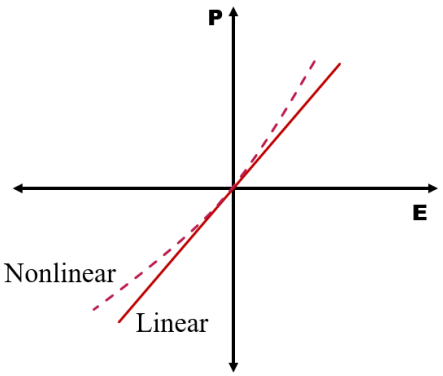

Fig. 2. Linear and nonlinear polarization responses to an applied electric field (E). The solid line is the linear case, and the dashed line is the nonlinear case.

Nonlinear susceptibility (χ) is a quantity used to measure a material's nonlinear polarization as a function of an applied electric field strength. The magnitude of NLO properties is determined not only by the intensity of the applied field but also by the NLO susceptibility coefficients (Popov et al., 2017). They describe a wide range of nonlinear optical effects based on the different orders of NLO susceptibility. The atomic field is comparable to the applied radiation field on the medium. Laser sources produce light with high intensities enough to change the materials' optical properties. The electron displacement is proportional to the order of polarization. As a result, the greater the displacement, the greater the NLO polarization response (Stucky et al., 1989). The nonlinearity is of electronic origin, and the nonlinear susceptibility is calculated using a simple order-of-magnitude appreciation of the magnitude of these quantities (Armstrong et al., 1962). Equation 3 represents the dependence of the induced higher-order polarization on the strength of the applied electric field and is considered the basis for all NLO phenomena (Burkins, 2017).

3. Third-order nonlinear optical properties

3.1. Nonlinear Absorption

Despite the fact that there are numerous NLO phenomena, we are most concerned with NLA and NLR. The photons of the incident light field are absorbed by molecules if their energy matches the energy of a transition between the ground and excited states of the molecules. NLA is a process in which light alters a material's optical absorptive properties (Van Stryland & Hagan, 2003). NLA changes a material's transmission as a function of intensity, or more precisely, irradiance. For increasingly intense laser beams, the likelihood of absorbing more than a single photon prior to relaxation to the ground state increases. NLA refers to the nonlinearities that cause famous optical effects like 2PA, three-photon absorption (3PA), FCA in solids, saturable absorption, and others (Kaiser & Garrett, 1961). Third-order optical nonlinearity manifests itself as a refractive index and absorption coefficient dependence on light beam intensity (Boyd). When it comes to absorption, the well-known Beer's law for linear absorption is as follows:

$$I_{(z)} = I_0 \, e^{-\propto(\omega)L} \tag{4}$$

Where I_0 is input intensity, $\propto(\omega)$ is the linear absorption coefficient, L represents the material thickness, and $I_{(z)}$ represents intensity at depth z. Beer's law is simply a differential equation solution that explains how light intensity decreases with propagation depth in a material when $\propto$ is constant.

$$\frac{\partial I}{\partial z} = - \propto (\omega) I \tag{5}$$

If multi-photon nonlinear effects are to be taken into consideration, this differential equation must be enlarged to include higher order intensity terms (Ganeev et al., 2004).

$$\frac{\partial I}{\partial z} = - \propto (\omega) I - \beta(\omega) I^2 - \gamma(\omega) I^3 - O(I^4) \tag{6}$$

Where $\beta(\omega)$ is the 2PA coefficient, $\gamma(\omega)$ is the 3PA coefficient, and $O(I^4)$ is the four-photon and higher absorption terms.

3.1.1. Two-Photon Absorption

Two-photon absorption 2PA is the absorption of two photons at the same time from incident laser beam, causing an electron to be excited from a lower to a higher (excited) state via an intermediate virtual state (2PA) (Tutt & Boggess, 1993). An electron in the ground state can be excited by two photons from a single beam of frequency ω or two photons from separate beams of frequencies ω_1 and ω_2. When a laser light with a frequency ω and an intensity of I passes in the medium, the two-photon effect can be produced. The two photons in this case, they have an equal frequency: $\omega_1 = \omega_2 = \omega$ (Said et al., 1992). And the corresponding two beams of light have $I_1 = I_2 = I$ and $\beta_1 = \beta_2 = \beta$. The 2PA process can be represented using a single equation, which is

$$\frac{\partial I}{\partial z} = -\beta(\omega)I^2 \tag{7}$$

If a material's linear absorption is negligible and 2PA dominates. This can be accomplished by separating variables which yield

$$I(L) = \frac{I_0}{1+\beta L I_0} \tag{8}$$

2PA causes much stronger absorption and thus more beam attenuation. This is due to the laser intensity dependence of NLA. Which shows the output intensity is smaller than the input intensity (I_o) and is affected by the 2PA coefficient (β) and the sample thickness (L) (Rumi & Perry, 2010). Figure 3 depicts the 2PA process in which one photon excites the carrier to a virtual state and, before it can relax, the carrier is excited by the absorption of another photon, hence the term two-photon absorption (Bernardo, 2020). The absorption of the two photons, both with energy ħω for a single beam configuration, is then considered instantaneous as the action takes place on a shorter time scale than the relaxation time from the virtual state (Kirilyuk et al., 2010). 2PA is related to the imaginary part of the $\chi^{(3)}$ coefficient (De Boni et al., 2003). The total absorption coefficient is given by $\alpha(I) = \alpha_0 + \beta I$, where the α_0 is the linear absorption coefficient and β is the 2PA coefficient, which is associated with the imaginary part of Im [$\chi^{(3)}$]:

$$\beta = \frac{6\omega}{\varepsilon_0 c^2 n^2} \text{ Im } [\chi^{(3)}] \tag{9}$$

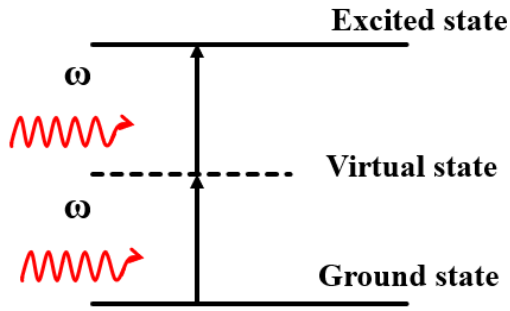

Fig. 3. Schematic diagram for the two-photon absorption process.

Two-photon fluorescence imaging (Denk et al., 1990a; So et al., 2000), two-photon microfabrication (Maruo et al., 1997a), and 3D optical data storage (J. H. Strickler & W. W. Webb, 1991) are all applications of 2PA processes. For optical limiters utilized in sensor protection, two photon absorbers are also required (Van Stryland et al., 1988a).

3.1.2. Saturable Absorption

Saturable absorption (SA) occurs when the transmission of a system increases at high excitation intensity. SA differs from two-photon absorbers only by having a real intermediate state and requiring the absorption cross section of the ground state to be larger than that of the excited state when interacting with intense light (Burkins, 2017). Many experiments show that when some materials are irradiated with a laser, their absorption coefficient decreases with increasing laser intensity until it reaches a saturation value recognized as SA. The total absorption coefficient α(I) related to the laser intensity I is described as follows (Szöke & Javan, 1963):

$$\alpha(I) = \frac{\alpha_0}{1+\frac{I}{I_{sat}}} \tag{10}$$

where the saturation intensity is I_{sat}, which varies depending on the material's property. In the 1970s, SA was widely used in laser-pulse compression techniques, including Q-switching and mode-locking (Hercher et al., 1968). The SA is explained by the energy-level transition model of different particles (molecules, ions, or atoms) of the medium under laser effect. The lower state particles absorb photon energy from the incident laser source and excite them to

higher states. If the laser is powerful sufficiently, it will cause the system's absorption to reach saturation, as depicted in Fig. 4.

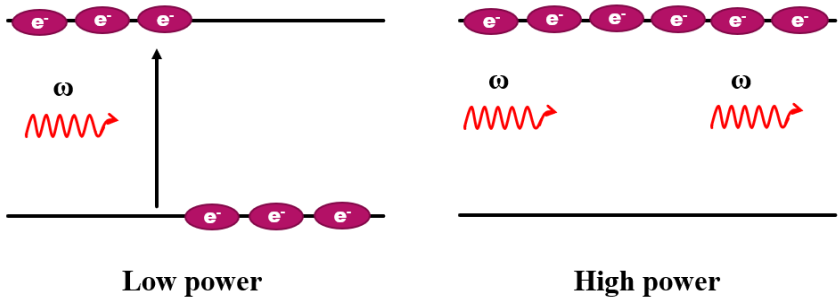

Fig. 4. Schematic diagram of saturable absorption.

Saturable absorbers are currently used primarily in laser passive mode-locking and Q switching (Hönninger et al., 1999).

3.1.3. Reverse saturable absorption

It is the same as saturable absorption, except that the absorption cross-sectional area of the excited state is larger than the ground state. In this case the transmission of the sample decreases, or the absorption increases with increasing laser intensity. RSA is a type of NLA produced by transitions between excited states in the presence of intense light radiation. The ground-state absorption is weak but excited-state absorption is strong, allowing for the generation of the RSA (Li, 2017a). The RSA process is depicted schematically in Figure 5. In the singlet system, S_0 is the ground-state level; S_1 and S_2 are the first and second excited-state levels. In the triplet system, T_1 and T_2 are the first and second excited-state levels, respectively. When the molecule system is irradiated with a laser beam of frequency ω, the molecules on ground state level S_0 absorb the photons at frequency ω and excite them to the levels S_1, S_2, and T_2 with the absorption cross sections σ_0, σ_S, and σ_T, respectively (Li, Zhang, Wang, et al., 1994; Li, Zhang, Yang, et al., 1994). The RSA, in which the absorption coefficient $(\alpha(I))$ increases with increasing light intensity, $\alpha(I) = \sigma n$, where σ is the absorption cross-section and n is the molecule-number density, the system's total absorption coefficient as expressed

$$\alpha(I) = \sigma_0 n_1 + \sigma_S n_2 + \sigma_T n_3 \quad (11)$$

The variation of molecule-number densities with time takes into consideration n_1, n_2, and n_3 at the energy levels S_0, S_1, and T_1.

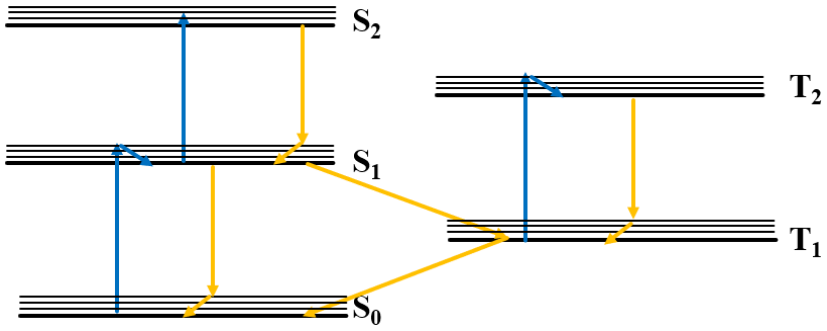

Fig. 5. Schematic diagram of reverse saturable absorption.

RSA can be used to create enhanced-absorption-type mirrorless devices, which are all-optical bistable devices (Li, Zhang, Yang, et al., 1994). Laser protection is another remarkable application of RSA, in which it is formed into NLO limiters to help protect human eyes or photodetectors from laser weapon damage (Li et al., 2000; Song et al., 1999).

3.2. Nonlinear Refraction

NLR is the process by which laser light alters a material's optical refractive properties. NLR causes optical effects like self-focusing (defocusing) and self-phase modulation. The refractive index of a coherent laser beam changes as it travels through a nonlinear medium. The variation in the refractive index is proportional to the light intensity (Günter et al., 1988). The optical Kerr effect (OKE) is a process that involves an intensity-dependent refractive index and is directly related to $\chi^{(3)}$. Electronic polarization, molecular reorientation, electrostriction, and thermal effects are all physical mechanisms that cause changes in refractive index (Sheik-Bahae & Hasselbeck, 2000).

3.2.1. Kerr Effect

The optical Kerr effect (OKE) is a process where the electric field of incident light causes a change in a medium's refractive index (Heiman et al., 1976). The magnitude of the change in refractive index is proportional to the square of the electric field strength or light intensity, $\Delta n \propto |E|^2 \propto I$. This effect relates to a third-

order NLO effect (Wong & Shen, 1974), and its nonlinear susceptibility is represented by $\chi^{(3)}$. When a high-intensity laser beam propagates through a medium with a large $\chi^{(3)}$ coefficient and the laser intensity has a Gaussian spatial distribution, the refractive index is greatest (Hanson et al., 1976). The medium will effectively serve as a positive lens, focusing the beam. This is the result of Kerr lensing (Shen, 1966). Assume a laser beam diffuses through a material. The OKE causes the material's refractive index to change Δn, and the phase change of the laser light for the propagation distance L is

$$\Delta\emptyset = k_0 \Delta n \, L = \frac{2\pi L}{\lambda_0} \Delta n \tag{12}$$

where λ_0 and k_0 are the excitation wavelength and wave vector of the laser in vacuum, respectively. That is, when a laser beam propagates through a material, the refractive-index change in the material can modulate the phase of the laser light. The n_2 change is proportional to the nonlinear phase change. Consequently, we can determine the refractive-index change of the medium Δn by detecting the light phase change $\Delta\emptyset$ (Hellwarth et al., 1971).

3.2.2. Self-phase modulation

When high-power laser light is an input into the nonlinear medium, the laser intensity produces the OKE, or a change in the medium's refractive index, which modulates the light's phase (Brabec & Krausz, 2000). This is known as self-phase modulation (SPM), also referred to as the self-action OKE. In the case of calculating the refractive index, the dielectric constant could be replaced with a uniform effective medium, ε (Li, 2017b). At a low optical field, the refractive index n_0 depends on both the linear dielectric, ε_1, and susceptibility, $\chi^{(1)}$, as illustrated in the following form (White, 2018): $\varepsilon_1 = 1 + \chi^{(1)}$, $n_0 = \sqrt{\varepsilon_1}$

$$n_0{}^2 = \varepsilon_1 = 1 + \chi^{(1)} \tag{13}$$

Effective susceptibility is defined as:

$$\chi = \chi^{(1)} + \chi^{(3)} |E|^2 \tag{14}$$

The general expression for studying the relationship between nonlinear susceptibility and the material refractive index change is as follows: (Franken et al., 1961; White, 2018):

$$n^2 = 1 + \chi\,(|E|^2) \tag{15}$$

$$n = (1 + \chi^{(1)} + \chi^{(3)}\,|E|^2)^{1/2} \tag{16}$$

$$\left(n_0{}^2 + \chi^{(3)}\,|E|^2\right)^{\frac{1}{2}} = n_0\left(1 + \frac{\chi^{(3)}\,|E|^2}{n_0{}^2}\right)^{\frac{1}{2}} \tag{17}$$

$$n = n_0 + \frac{\chi^{(3)}\,|E|^2}{2\,n_0{}^2} = n_0 + \frac{n_2\,|E|^2}{2} \tag{18}$$

The first item in Eq. (18) is a linear refractive index, the second is a n_2 and the nonlinear refractive index is

$$n = n_0 + n_2\,\langle E.E\rangle = n_0 + \Delta n \tag{19}$$

In the SPM effect, the Δn is proportional to the laser light intensity, and the n_2 is proportional to the real part of the $\chi^{(3)}$ (Hendry et al., 2010).

3.2.3. Self-focusing and self-defocusing

When a laser light passes through a material, because the laser beam has a Gaussian intensity distribution, the intensity at the center is much greater than the intensity at the edge (Li, 2017b). As previously stated, the Δn is relative to the intensity of laser light I, $\Delta n = n_2 I$. The refractive-index distribution of the medium becomes non-uniform along the radial direction as a result of the OKE. The nonlinear material in this case acts like a lens, causing the laser beam's profile size to change continuously, either through convergence or divergence, as illustrated in Fig. 6. When $n_2 > 0$, the medium exhibits the convex lens effect, focusing the light beam; this is known as self-focusing; when $n_2 < 0$, the medium exhibits the concave lens effect, defocusing the laser light, this is referred to as self-defocusing. In the self-focusing case, the Gaussian laser beam intensity gradually decreases along the radial direction of the medium from the axes to the beam's edge. As a result, the medium's refractive index $n = n_o + n_2 I$ gradually decreases along the radial direction (Bergé, 1998).

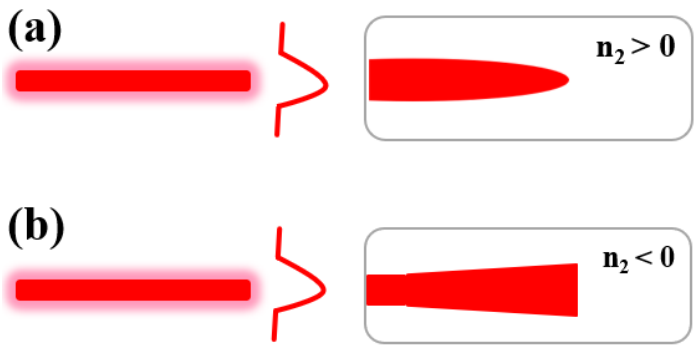

Fig. 6. Schematic diagram of a Gaussian laser beam propagating in the nonlinear medium, (a) self-focusing ($n_2 > 0$); (b) self-defocusing ($n_2 < 0$).

4. Z-scan technique

The Z-scan technique is the one of the most well-known techniques for measuring the NLO properties of all kinds of media. Most of the previous measurement methods require the use of more than two incident light beams and are incapable of directly measuring the real and imaginary parts of susceptibility (Kelley, 1965; Sheik-Bahae et al., 1989a). People discovered a Z-scan method that relied on self-focusing at the end of the twentieth century (Sheik-Bahae et al., 1990). This method not only measures susceptibility with a single light beam but also measures the real and imaginary components of susceptibility. A single experimental setup can be utilized to determine the value and sign of the n2 and the β. This method can be used to quickly determine whether a material's nonlinear refraction is self-focusing or self-defocusing, or whether it has saturable or reverse saturable absorption (Gu & Wang, 2011). The main experimental tool utilized in this study is the Z-scan method to measure thermal nonlinear properties.

4.1. The Z-scan measurements

The Z-scan technique, developed by E.W. Van Stryland, his graduate student M. Sheik-Bahae, and their colleagues in 1990 (Sheik-Bahae et al., 1989a), is one of the more common techniques for measuring NLA and NLR. It is used to investigate many materials including semiconductors, biological materials, and liquid crystals (Ule, 2015). In this technique, the optical transmittance of the nonlinear material is determined as the sample passes through the focus of a

Gaussian beam. Their method can measure both the sign and magnitude of the n2 with sensitivity comparable to interferometric methods, as well as the β (Sheik-Bahae et al., 1990). NLA information is obtained by gathering all the transmitted power, whereas NLR data is obtained by gathering the transmitted power through an aperture centered on the beam in the far field. The Z-scan is a predominant technique due to its simplicity, sensitivity, accuracy, and ease of separating NLA and NLR. This discovery was motivated by the need to characterize the value of materials' $\chi^{(3)}$ for applications such as all optical switching and optical limiting. The basic principle of Z-scan involves translating a sample through the focal point of a sharply focused beam of laser light. Z-scan measurement techniques are divided into two types: CA and OA. The CA Z-scan technique measures the n_2, whereas the OA Z-scan technique measures the β of the material, as depicted in Fig. 7. For the OA Z-scan, all the light transmitted through the sample is captured by the detector (D1), allowing for the measurement of the intensity dependent change in transmission. In CA Z-scan, a small aperture is put between the sample and the detector, which detects the material's self-focusing or self-defocusing properties. The Z-scan method, in essence, measures the transmitted laser intensity of a nonlinear material in the far field. The transmittance of a sample varies with its position in relation to the focal point of a lens (Badran & Al-Fregi, 2012; Sheik-Bahae et al., 1990). The Z-scan is now the most widely used method for measuring thermal and optical nonlinearities.

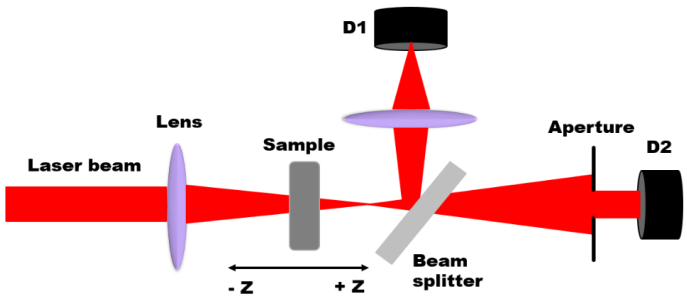

Fig. 7. Basic CA and OA Z-scan experimental setup. The beam splitter allows an OA Z-scan to be recorded concurrently. Detector D2 collects the CA data and detector D1 collects the OA data.

The laser beam strikes the sample. The sample is put on a translation stage and moved through the beam waist, the most focused region of the beam,

generally beginning near the focusing lens and moving away in the positive z direction. The beam exits the sample and is split in two; in the case of OA Z-scan, the reflected expanding beam is focused directly into detector D1, while in the case of CA Z-scan, the transmitted portion traverses a pinhole aperture in the far field to finally strike detector D2.

4.1.1. Closed aperture

Because distortion of the laser beam phase is converted to amplitude distortion through propagation from the sample to the far field, putting an aperture centered on the beam in the far field in front of a detector makes the detector sensitive to phase distortion, this is known as a CA Z-scan (Sheik-Bahae et al., 1991). The irradiance increases as the sample moves from a distance before the focus (negative z) to the focus, causing self-lensing in the sample. Positive/negative self-lensing tends to broaden/narrow the beam at the aperture prior to focusing, resulting in a decrease/increase in measured transmittance (Balu, 2006). Consider a material with a positive n_2 and a thickness is less than the diffraction length of the focused Gaussian beam. Starting the scan from a distance before the focus (i.e., the prefocal region, -z), the nonlinear medium will focus the beam earlier and to a small waist. Since the beam waist is reduced, the beam expands more rapidly due to diffraction as shown in Fig. 8. Therefore, in the near field, the beam remains collimated over a shorter distance and diverges at a larger beam angle in the far field. The overall effect is a reduction in the intensity at the detector (Günter, 2012). When the sample passes into the postfocal region (+z), the positive self-lensing of the nonlinear material tends to reduce the beam divergence, resulting in increased intensity at the detector. For a material with a negative n_2, the reverse explanation applies. The difference in behavior shown by positive and negative n_2 can thus provide a unique signature of the sign of the nonlinearity (Philip et al., 2000). A positive nonlinearity ($n_2>0$) is defined by a prefocal transmittance minimum followed by a postfocal maximum, whereas a negative nonlinearity ($n_2<0$) is defined by a prefocal maximum followed by a minimum. Fig. 9 shows the simulated CA Z-scan profile.

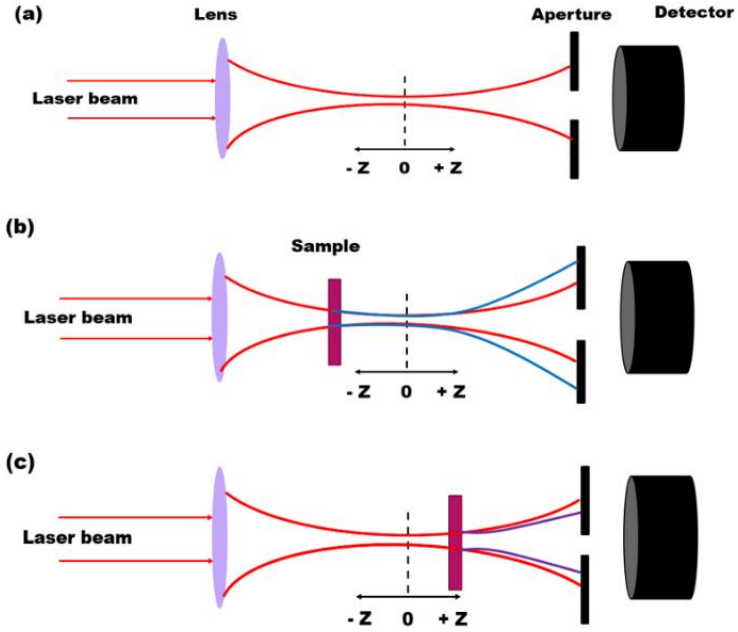

Fig. 8. A schematic diagram of a CA Z-scan setup (a) laser beam propagation without sample, (b) a sample in the prefocal position, the beam would expand further in the far field than if the medium wasn't present. This creates a dip or valley in the transmission as less light gets through the aperture. (c) In the postfocal position, the beam is focused to allow more light to pass through the aperture. The transmission accessed by the detector will then become larger, generating the peak in the signal.

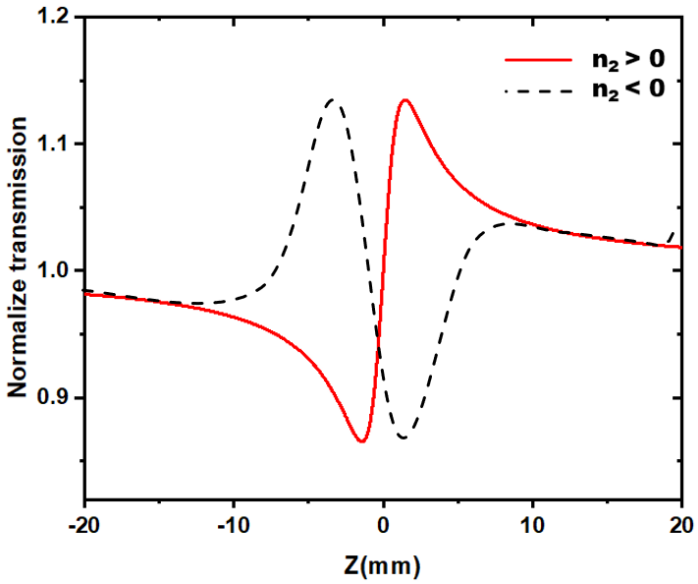

Fig. 9. An ideal CA Z-scan curve transmittance versus sample position. A solid curve represents material that shows self-focusing, positive phase shift, and a positive n_2. The dashed curve depicts self-defocusing, a negative phase shift, and negative n_2.

Not only is the sign of n_2 investigates from a Z-scan, but also its magnitude, which can be easily determined utilizing a simple analysis for a thin medium. Similarly, β can also be calculated by assuming a TEM_{00} Gaussian beam with a waist radius of w_0 traveling in the +z direction. The electric field can be expressed as follows (Kim & Kwak, 2009; Kogelnik & Li, 1966):

$$E\,(z,r,t) = E_0\,(t)\frac{\omega_0}{\omega_{(z)}}.\exp\left(-\frac{r^2}{\omega^2(z)}-\frac{ikr^2}{2R(z)}\right)e^{-i\emptyset(z,t)} \tag{20}$$

where $\omega^2(z) = {\omega_0}^2\,(1+\frac{z^2}{z_0^2})$ is the beam radius, $R_{(z)} = z(1+\frac{z^2}{z_0^2})$ is the radius of curvature of the wavefront at z, $z_0 = k{\omega_0}^2/2$, is the diffraction/Rayleigh length of the beam, $k = 2\pi/\lambda$ is the excitation wavelength, all in free space. $E_0\,(t)$ is the radiation electric field measured at focus and it includes the laser pulse's temporal envelope. $E^{-i\emptyset(z,t)}$ contains the radially uniform phase variations. The amplitude and phase of the electric field for a thin nonlinear sample are defined by the slowly varying envelope approximation and are expressed by the following pair of equations (Hermann, 1992):

$$\frac{d\Delta\emptyset}{dL} = \frac{2\pi}{\lambda}\,\Delta n(I) \tag{21}$$

$$\frac{dI}{dL} = -\propto(I)I \tag{22}$$

where L is the propagation length in the sample. There is insufficient path length ($\Delta\emptyset$) in a thin nonlinear refractor for the beam to change size as it propagates through the medium. The nonlinearity causes a phase change in the nonlinear medium. Therefore, for material with cubic nonlinearity and negligible β, the phase shift at the exit end of the sample can be determined by solving Eqs.(21) and (22). This is expressed as (Sheik-Bahae et al., 1990):

$$\Delta\emptyset(z,r,t) = \Delta\emptyset_0(z,t)\exp\left(-\frac{2r^2}{\omega^2\,(z)}\right) \tag{23}$$

The on-axis phase shift at the focus is

$$\Delta\emptyset_0(t) = k\Delta n_0(t)L_{eff} \tag{24}$$

where the effective length of the sample

$$L_{eff} = (1 - e^{-\propto L})/\propto \quad (25)$$

And $\Delta n_0 = n_2 I_0$, where I_0 is the on-axis intensity at focus (z=0), $I_0 = \frac{P}{\pi \omega_0{}^2}$, P is the incident power within the sample. The electric field at the sample's exit end Ee contains information about the beam's nonlinear phase shift. This is written as (Weaire et al., 1979):

$$E_e\,(z, r, t) = E\,(z, r, t)\, e^{-\propto L/2}\, e^{i\emptyset(z,t)} \quad (26)$$

The power transmitted at the aperture plane PT ($\Delta\emptyset_0(t)$) can be obtained by spatially integrating the resultant electric field pattern at the aperture, $E_a(r, t)$, up to the aperture radius r_a. The normalized Z-scan transmitted power can be determined as follows (Liu & Tomita, 2012; Weaire et al., 1979):

$$T(z,t) = c\varepsilon_0 n_0 \pi \frac{\int_{-\infty}^{\infty}\int_0^{r_a} |E_a(r,t)|^2\, r dr dt}{S\int_{-\infty}^{\infty} P_i(t) dt} \quad (27)$$

with S denoting the transmittance of the aperture in the linear regime. The far-field output of an aperture detector is used to measure the normalized transmittance, which can be given as (Liu & Tomita, 2012):

$$T(z, \Delta\emptyset_0) = 1 - \frac{4\Delta\emptyset_0\, z/z_0}{\left(\left(\frac{z}{z_0}\right)^2 + 9\right)\left(\left(\frac{z}{z_0}\right)^2 + 1\right)} \quad (28)$$

The extrema (peak and valley) of the on-axis Z-scan transmittance can also be calculated for small phase distortions ($|\Delta\emptyset_0| \ll 1$) and small apertures (S ~ 0) by solving the equation: $dT(z, \Delta\emptyset_0) / dz = 0$ =. The result is obtained by the relation (Sheik-Bahae et al., 1990):

$$\Delta T_{p-v} = 0.406|\Delta\emptyset_0| \quad (29)$$

Using Eq. (24), we can estimate the nonlinear refractive index:

$$\Delta n = \frac{\Delta T_{p-v}}{0.406|\Delta\emptyset_0|} \quad (30)$$

When the aperture is larger but the phase variation at the focal point $|\Delta\emptyset_0| \leq \pi$,

$$\Delta T_{p-v} = 0.406(1 - S)^{0.25}|\Delta\emptyset_0| \quad (31)$$

In this case, the formula of nonlinear refractive index is

$$\Delta n = \frac{\Delta T_{p-v}}{0.406(1-S)^{0.25}|\Delta\emptyset_0|} \quad (32)$$

This transmission equation (28) applies to the CA Z-scan measurements in this thesis for a Gaussian beam and extracts the nonlinear refractive indices for the material.

4.1.2. Open aperture

OA Z-scan is considered simpler to analyze than CA Z-scan. This is because the overall transmission through the sample is measured when the aperture prior to the detector is removed (Zheng et al., 2015). For the measurement of the β, the same experimental setup is utilized but with a wide-open aperture as shown in Fig. 10 Linear absorption takes place when an electron is excited with one photon to an excited level, whereas NLA takes place when an electron is excited with two or more photons with energy equal to the exciting level, as shown in Fig. 10 (Al Abdulaal, 2016). The 2PA effect in the OA Z-scan method is intensity dependent; as the intensity of the Gaussian beam increases at focus, the 2PA effect increases. The NLA increases as the material is moved closer to the focus (Badran & Al-Fregi, 2012).

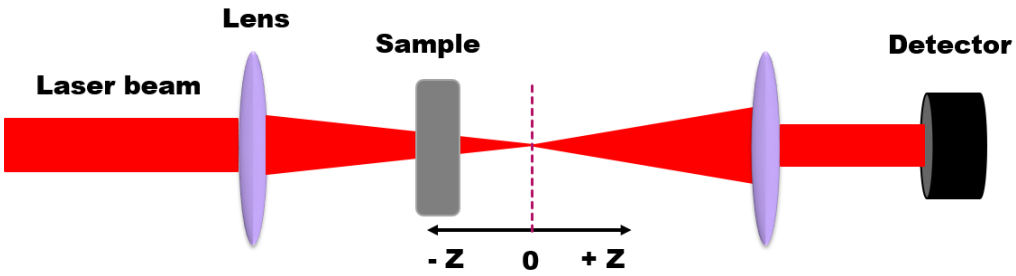

Fig. 10. Schematic diagram of a typical OA Z-scan set up.

The nonlinear absorption of medium is measured in the Z-scan method at some z point in the light propagation direction, $\propto (z, r) = \propto_0 + \beta I(z, r)$. When $\beta < 0$, it is SA; when $\beta > 0$, it is RSA or 2PA (Li et al., 2018). As shown in Fig. 11, the SA experimental curve is a symmetrical peak curve with maximum transmittance

at the centre of the focal point position; the RSA curve is a symmetrical valley curve with minimum transmittance at the centre of the focal point position.

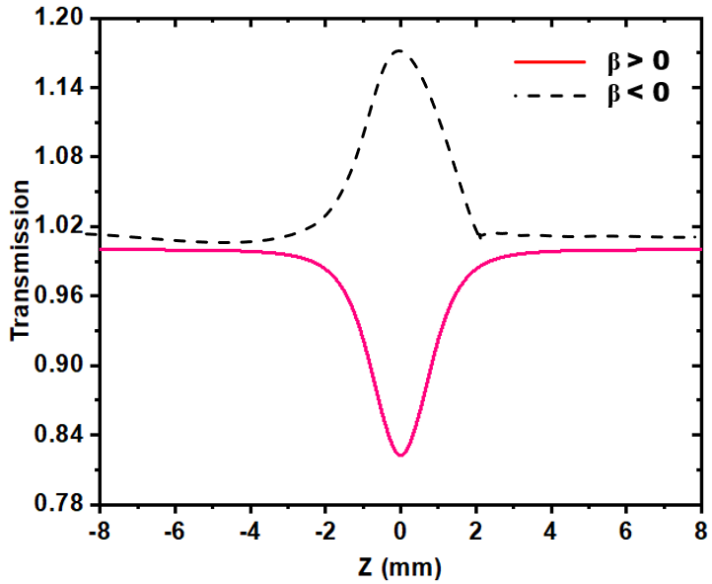

Fig. 11. Normalized transmission as a function of z-position in the open aperture Z-scan technique. A solid curve represents a material that shows reverse saturable absorption ($\beta > 0$). The dashed curve depicts saturable absorption ($\beta < 0$).

For NLA measurements using the OA Z-scan technique, equations (21) and (22) were solved with free-carrier effects (refractive and absorptive) ignored to obtain the light intensity and phase shift at the exit surface as (Sheik-Bahae et al., 1990):

$$I_e(z, r, t) = \frac{I_0\,(r,z,t)\; e^{[-\propto(I)L]}}{1+q(r,z,t)} \tag{33}$$

and

$$\Delta\emptyset(z, r, t) = \frac{kn_2}{\beta} \ln[1 + q(z, r, t)], \tag{34}$$

where

$$q(z, r, t) = \beta I(z, r, t) L_{eff} \tag{35}$$

The complex field amplitude on outputted surface of sample can be expressed as (Kim & Kwak, 2009):

$$E_e(z,r,t) = E(z,r,t)e^{-\propto\frac{L}{2}}(1+q)^{\left(L\frac{kn_2}{\beta}-\frac{1}{2}\right)} \quad (36)$$

By the y integral of Eq. (33), the transmitted power is obtained as (Chapple et al., 1997):

$$P(z,t) = P_I(t)e^{-\propto L}\frac{\ln[1+q_0(z,t)]}{q_0(z,t)} \quad (37)$$

Where $P_I(t)$ is the input power, $P_I(t) = \pi\omega_0^2 I_0/2$, and q_0 is the complex parameter that is related to the β by (H. Li et al., 2001):

$$q_0(z,t) = \beta I_0 L_{eff}/\left(1+\left(\frac{z}{z_0}\right)^2\right) \quad (38)$$

The theoretical equation for fitting the normalized transmittance of an OA Z-scan in the far field is as follows: (Sheik-Bahae et al., 1990):

$$T_{OA} = 1 \pm \frac{q_0}{2\sqrt{2}}\frac{1}{\left(1+\left(\frac{z}{z_0}\right)^2\right)} \quad (39)$$

The normalized transmittance T_{OA} is defined as the sample transmittance at z position divided by the transmittance of the sample away from the focus. The material position in relation to the lens focus is represented by z, and the Rayleigh length is represented by z_0.

5. Linear and nonlinear optical properties of ITO films

TCO have high transparency at visible wavelengths as well as electrical conductivity comparable to that of metals (Hosono et al., 2002). TCOs are binary or ternary compounds including one or two metallic elements (Mattox & Mattox, 2007). TCO thin films have actual and potential applications such as transparent electrodes for flat panel displays, low emissivity windows, transparent thin film transistors, light emitting diodes, and semiconductor lasers (Barquinha et al., 2012; Mei et al., 2013; Mlyuka et al., 2009; Pan et al., 2001; Razeghi, 2002). One of many TCOs that are widely used in practical optoelectronic devices is ITO (Guo et al., 2019a; Park, Kim, Lee, Kim, & Lee, 2010). ITO films have received a lot of attention in comparison to other transparent conducting oxides (Minami, 2005). ITO is a solid solution of indium (III) oxide (In_2O_3) and tin (IV)

oxide (SnO_2), with approximately 90% wt. In_2O_3 and 10% wt. SnO_2. It is colorless and transparent as a thin film and yellowish to grey as a bulk material (Stadler, 2012). The general chemical formula of ITO thin film is $In_4Sn_3O_{12}$, and it has low electrical resistivity, high optical transparency (over 80%) in the visible wavelength range, and high reflection in the infrared (A. Eshaghi & A. Graeli, 2014; Ma et al., 2021a). ITO is an electrically conductive material made up of In_2O_3 doped with Sn, which replaces the In^{3+} atoms in the crystal lattice structure of In_2O_3 to enhance the conductivity (Nadaud et al., 1998a; Pokaipisit et al., 2007). ITO's strong conductivity is due to both substitutional tin and oxygen vacancies (Giusti, 2011; Ma et al., 2015a). The ITO film is an n-type semiconductor with a band-gap greater than 3 eV, and it is used in many applications (Ishibashi et al., 1990; Pokaipisit et al., 2008). Because of these properties, ITO is widely used in many fields, including optics and electronics (Bel Hadj Tahar et al., 1998; Manoj et al., 2007). Figure 12 depicts doping sites for tin (Sn) in In_2O_3 lattice (Y. Li et al., 2001). The Sn atom occupies an interstitial site and donates an electron, converting doped indium oxide to indium tin oxide.

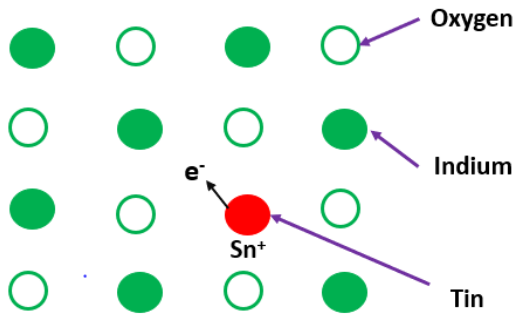

Fig. 12. Sn doping sites in an In_2O_3 lattice.

Fig. 13 depicts the undoped and Tin (Sn) doped indium oxide band structure. Sn^{4+} Substitutes In^{3+} and introduces dopant energy levels just below the conduction band (CB) in In_2O_3. The excess electrons are easily activated as free carriers in the CB, resulting in a significant rise in conductivity. The Fermi level rises into the CB as doping increases, and the materials eventually exhibit degenerately doped semiconductor or free electron-like metallic behavior. In their first attempt to describe ITO, Fan and Goodenough (J. C. Fan & J. B. Goodenough, 1977) suggested the model of schematic energy band structure for

In_2O_3 and ITO, which helps a qualitative explanation of the apparent high optical transparency and electrical conductivity, as shown in Fig. 13. In Fan's band model, In_2O_3 has a large direct band gap (3.5 eV), preventing interband transitions in the visible range and so creating transparency within this frequency range, which is still the reference model for ITO today. Indium 5s orbitals are thought to form the conduction band, while oxygen 2p electrons are thought to form the valence band. Because of n-type doping of the Sn impurities, the Ef is found a few eV below the conduction band (Giusti, 2011). Donor states at low doping density form below the conduction band, and the Ef is located between the minimum of the conduction band and the donor level. Donor density, on the other hand, increases as doping levels rise.

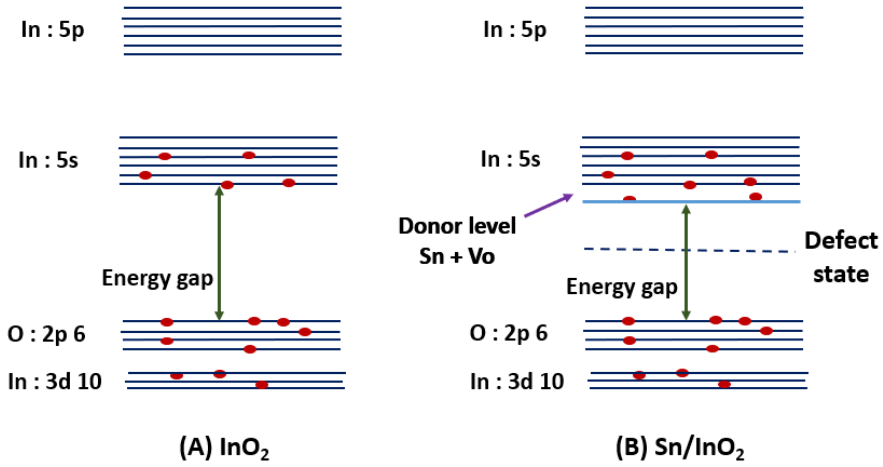

Fig. 13. Electronic band structure of In_2O_3 and Sn doped In_2O_3.

Some studies (P. Guo, R. D. Schaller, J. B. Ketterson, & R. P. Chang, 2016; Khurgin et al., 2020a; Xiao et al., 2020a; Zhang et al., 2019) studied the linear and NLO properties of ITO utilizing various measuring techniques, where the ITO was prepared in various shapes and sizes using various preparation methods. Kumar et al. (Kumar et al., 2013) studied the NLO properties of a gold cluster on ITO using an 80-fs laser with a wavelength of 395 nm. Tingzhen et al. (Yan et al., 2022) used a 1 MHz and 80 fs laser with a wavelength of 1550 nm to investigate the nonlinear absorption of ITO/PVA composite materials. Tarek Mohamed et al. (Ali et al., 2020) measured the NLO properties of ITO thin film using a 100 fs and an 80 MHz laser with excitation wavelengths ranging from

720 to 900 nm. Many fantastic NLO effects of ITO film have recently been exploited, including nonlinear absorption, Kerr nonlinearity (Kinsey et al., 2015a), and four-wave mixing. Because optical Kerr nonlinearity has a direct impact on all-optical switching devices, the Kerr nonlinearity effect is responsible for the self-focusing phenomenon and the self-phase modulation, which are among the most fascinating and intensely researched. In (Humphrey & Kuciauskas, 2006), the $\chi^{(3)}$ of ITO was discovered to be purely electronic in the NIR region using femtosecond laser pulses. The experimental results of (Humphrey & Kuciauskas, 2006) proved the n_2 depends on carrier concentration and excitation wavelength, 200 fs laser pulses, and 1 kHz repetition rate.

6. Application of ITO

ITO is the most commonly utilized and evolved TCO material, and it is still considered the "gold standard" of TCOs. At the end of the 1960s, TCO materials were widely used in industry, when IR light filters made of Tin or In_2O_3 were utilized on low-pressure sodium discharge lamps to increase lamp efficiency by minimizing heat losses (Köstlin et al., 1975; Mcmaster, 1947). After that, with the introduction of flat-panel display technology in the1970, ITO became the most widely used TCO material for transparent electrodes with the lowest resistivity (i.e., order of 1–2 × 10^{-4} Ω·cm) (Betz, Olsson, Marthy, Escolá, & Atamny, 2006; Katayama, 1999). Due to its high electrical conductivity and transparency, ITO has been widely utilized as a transparent electrode in the solar industry and photovoltaic applications. The significant technological advancements that have enabled this growth are discussed in chronological order. ITO has unique NLO properties and applications (P. Guo, R. D. Schaller, L. E. Ocola, et al., 2016). Nonlinear optical processes in ITO have demonstrated fundamental research importance as well as technological implications in a wide range of NLO applications, such as optical limiting, nonlinear integrated photonic devices, multiphoton processes, two-photon lasing and detection, and numerous other nonlinear optics avenues that can potentially be utilized in NLO devices. ITO has several NLO applications that are unique.

7. Conclusion

Nonlinear optical responses of materials are important topics for applications including quantum information processing. This review is given on the recent developments in the studies of nonlinear optical responses in ITO semiconductor materials. The geometric nature of the electronic states in semiconductors plays a crucial role in the enhancement of the nonlinear optical properties of these materials. Because of developments in NLO phenomena such as third-order susceptibility, measuring the nonlinearity of materials is very important. Nonlinear parameters such as n_2 and β have been measured using different techniques. However, the Z-scan has been widely regarded as the standard method due to its ease of use and sensitivity. The previous studies confirmed that ITO thin film has many potential applications, including photonics and optoelectronics, due to its high nonlinear absorption coefficient.

Funding This research received no external funding.

Data availability No datasets were generated or analysed during the current study.

Declarations

Conflict of interest The authors declare no conflict of interest.

Competing interests The authors declare no competing interests.

References

Adair, R., Chase, L., & Payne, S. A. J. J. B. (1987). Nonlinear refractive-index measurements of glasses using three-wave frequency mixing. *JOSA B*, *4*(6), 875-881.

Afre, R. A., Sharma, N., Sharon, M., & Sharon, M. J. R. o. a. m. s. (2018). Transparent conducting oxide films for various applications: A review. *53*(1), 79-89.

Al Abdulaal, T. (2016). *Measuring Nonlinear Properties of Graphene Thin Films Using Z-Scan Technique*. University of Arkansas.

Alam, M. Z., De Leon, I., & Boyd, R. W. J. S. (2016). Large optical nonlinearity of indium tin oxide in its epsilon-near-zero region. *352*(6287), 795-797.

Ali, M., Shehata, A., Ashour, M., Tawfik, W. Z., Schuch, R., & Mohamed, T. (2020). Measuring the nonlinear optical properties of indium tin oxide thin film using femtosecond laser pulses. *JOSA B*, *37*(11), A139-A146.

Armstrong, J., Bloembergen, N., Ducuing, J., & Pershan, P. S. (1962). Interactions between light waves in a nonlinear dielectric. *Physical review*, *127*(6), 1918.

Arun Kumar, R. (2013). Borate crystals for nonlinear optical and laser applications: a review. *Journal of Chemistry*, *2013*.

Ashour, M., Abdel-Wahab, M. S., Shehata, A., Tawfik, W. Z., Azooz, M., Elfeky, S. A., & Mohamed, T. J. J. B. (2022). Experimental investigation of linear and third-order nonlinear optical properties of pure CuO thin film using femtosecond laser pulses. *JOSA B*, *39*(2), 508-518.

Asobe, M., Suzuki, K. i., Kanamori, T., & Kubodera, K. i. J. A. P. L. (1992). Nonlinear refractive index measurement in chalcogenide-glass fibers by self-phase modulation. *60*(10), 1153-1154.

Badran, H. A., & Al-Fregi, A. (2012). Synthesis and study of nonlinear optical properties of a new azo dye by Z-Scan technique. *IJSST*, *2*, 26-36.

Balu, M. (2006). *Experimental techniques for nonlinear material characterization: A nonlinear spectrometer using a white-light continuum Z-scan*. University of Central Florida.

Barquinha, P., Martins, R., Pereira, L., & Fortunato, E. (2012). *Transparent oxide electronics: from materials to devices*. John Wiley & Sons.

Bel Hadj Tahar, R., Ban, T., Ohya, Y., & Takahashi, Y. (1998). Tin doped indium oxide thin films: Electrical properties. *Journal of Applied Physics*, *83*(5), 2631-2645.

Benoy, M., Mohammed, E., Suresh Babu, M., Binu, P., & Pradeep, B. J. B. J. o. P. (2009). Thickness dependence of the properties of indium tin oxide (ITO) FILMS prepared by activated reactive evaporation. *39*, 629-632.

Bergé, L. (1998). Wave collapse in physics: principles and applications to light and plasma waves. *Physics reports*, *303*(5-6), 259-370.

Bernardo, C. R. d. F. (2020). Linear and non-linear optical properties owing to interactions of elementary excitations in nanostructures.

Betz, U., Olsson, M. K., Marthy, J., Escolá, M., & Atamny, F. (2006). Thin films engineering of indium tin oxide: large area flat panel displays application. *Surface and Coatings Technology*, *200*(20-21), 5751-5759.

Betz, U., Olsson, M. K., Marthy, J., Escolá, M., Atamny, F. J. S., & Technology, C. (2006). Thin films engineering of indium tin oxide: large area flat panel displays application. *200*(20-21), 5751-5759.

Boyd, R. Nonlinear Optics, Academic Press, San Diego 1992. *P. S. Pershan. Phys. Rev.*, *121*, 1963.

Brabec, T., & Krausz, F. (2000). Intense few-cycle laser fields: Frontiers of nonlinear optics. *Reviews of Modern Physics*, *72*(2), 545.

Burkins, P. J. (2017). *Femtosecond Z-scan measurements in novel materials with emphasis on managing thermal effects*. University of Maryland, Baltimore County.

Chapple, P., Staromlynska, J., Hermann, J., Mckay, T., & McDuff, R. (1997). Single-beam Z-scan: measurement techniques and analysis. *Journal of Nonlinear Optical Physics & Materials*, *6*(03), 251-293.

Clerici, M., Kinsey, N., DeVault, C., Kim, J., Carnemolla, E. G., Caspani, L., Shaltout, A., Faccio, D., Shalaev, V., & Boltasseva, A. J. N. c. (2017). Controlling hybrid nonlinearities in transparent conducting oxides via two-colour excitation. *8*(1), 1-7.

Correa, D. S., Cardoso, M. R., Tribuzi, V., Misoguti, L., & Mendonca, C. R. J. I. J. o. S. T. i. Q. E. (2011). Femtosecond laser in polymeric materials:

microfabrication of doped structures and micromachining. *18*(1), 176-186.

Coutts, I., Li, X., Wanlass, M., Emery, K., & Cessert, T. J. L. (1990). IEEE Electron. *26*, 660.

De Boni, L., Constantino, C., Misoguti, L., Aroca, R., Zilio, S. C., & Mendonça, C. R. (2003). Two-photon absorption in perylene derivatives. *Chemical physics letters, 371*(5-6), 744-749.

Denk, W., Strickler, J. H., & Webb, W. W. (1990a). Two-photon laser scanning fluorescence microscopy. *Science, 248*(4951), 73-76.

Denk, W., Strickler, J. H., & Webb, W. W. J. S. (1990b). Two-photon laser scanning fluorescence microscopy. *248*(4951), 73-76.

Diels, J.-C., & Rudolph, W. (2006). *Ultrashort laser pulse phenomena*. Elsevier.

Elim, H. I., Yang, J., Lee, J.-Y., Mi, J., & Ji, W. J. A. p. l. (2006). Observation of saturable and reverse-saturable absorption at longitudinal surface plasmon resonance in gold nanorods. *88*(8), 083107.

Eshaghi, A., & Graeli, A. (2014). Optical and electrical properties of indium tin oxide (ITO) nanostructured thin films deposited on polycarbonate substrates "thickness effect". *Optik, 125*(3), 1478-1481.

Eshaghi, A., & Graeli, A. J. O. (2014). Optical and electrical properties of indium tin oxide (ITO) nanostructured thin films deposited on polycarbonate substrates "thickness effect". *125*(3), 1478-1481.

Fan, J. C., & Goodenough, J. B. (1977). X-ray photoemission spectroscopy studies of Sn-doped indium-oxide films. *Journal of Applied Physics, 48*(8), 3524-3531.

Fan, J. C., & Goodenough, J. B. J. J. o. A. P. (1977). X-ray photoemission spectroscopy studies of Sn-doped indium-oxide films. *48*(8), 3524-3531.

Franken, P., Hill, A. E., Peters, C. e., & Weinreich, G. (1961). Generation of optical harmonics. *Physical Review Letters, 7*(4), 118.

Gabler, T., Waldhäusl, R., Bräuer, A., Michelotti, F., Hörhold, H.-H., & Bartuch, U. J. A. p. l. (1997). Spectral broadening measurements in poly (phenylene vinylene) polymer channel waveguides. *70*(8), 928-930.

Ganeev, R., Kulagin, I., Ryasnyansky, A., Tugushev, R., & Usmanov, T. (2004). Characterization of nonlinear optical parameters of KDP, LiNbO3 and BBO crystals. *Optics communications, 229*(1-6), 403-412.

Giusti, G. (2011). *Deposition and characterisation of functional ITO thin films* University of Birmingham].

Grehn, M., Seuthe, T., Tsai, W.-J., Höfner, M., Achtstein, A. W., Mermillod-Blondin, A., Eberstein, M., Eichler, H. J., & Bonse, J. J. O. M. E. (2013). Nonlinear absorption and refraction of binary and ternary alkaline and alkaline earth silicate glasses. *3*(12), 2132-2140.

Gu, B., & Wang, H.-T. (2011). Linear and Nonlinear Optical Properties of Ferroelectric Thin Films. In *Ferroelectrics-Physical Effects*. IntechOpen.

Günter, P. (2012). *Nonlinear optical effects and materials* (Vol. 72). Springer.

Günter, P., Huignard, J.-P., & Glass, A. M. (1988). *Photorefractive materials and their applications* (Vol. 1). Springer.

Guo, P., Schaller, R. D., Ketterson, J. B., & Chang, R. P. (2016). Ultrafast switching of tunable infrared plasmons in indium tin oxide nanorod arrays with large absolute amplitude. *Nature Photonics*, *10*(4), 267-273.

Guo, P., Schaller, R. D., Ketterson, J. B., & Chang, R. P. J. N. P. (2016). Ultrafast switching of tunable infrared plasmons in indium tin oxide nanorod arrays with large absolute amplitude. *10*(4), 267-273.

Guo, P., Schaller, R. D., Ocola, L. E., Diroll, B. T., Ketterson, J. B., & Chang, R. P. (2016). Large optical nonlinearity of ITO nanorods for sub-picosecond all-optical modulation of the full-visible spectrum. *Nature communications*, *7*(1), 1-10.

Guo, Q., Cui, Y., Yao, Y., Ye, Y., Yang, Y., Liu, X., Zhang, S., Liu, X., Qiu, J., & Hosono, H. J. A. M. (2017). A solution-processed ultrafast optical switch based on a nanostructured epsilon-near-zero medium. *29*(27), 1700754.

Guo, Q., Pan, J., Li, D., Shen, Y., Han, X., Gao, J., Man, B., Zhang, H., & Jiang, S. (2019a). Versatile mode-locked operations in an Er-doped fiber laser with a film-type indium tin oxide saturable absorber. *Nanomaterials*, *9*(5), 701.

Guo, Q., Pan, J., Li, D., Shen, Y., Han, X., Gao, J., Man, B., Zhang, H., & Jiang, S. J. N. (2019b). Versatile mode-locked operations in an Er-doped fiber laser with a film-type indium tin oxide saturable absorber. *9*(5), 701.

Guo, Q., Yao, Y., Luo, Z.-C., Qin, Z., Xie, G., Liu, M., Kang, J., Zhang, S., Bi, G., & Liu, X. J. A. n. (2016). Universal near-infrared and mid-infrared optical modulation for ultrafast pulse generation enabled by colloidal plasmonic semiconductor nanocrystals. *J ACS nano*, *10*(10), 9463-9469.

Hales, J. M., Matichak, J., Barlow, S., Ohira, S., Yesudas, K., Brédas, J.-L., Perry, J. W., & Marder, S. R. J. S. (2010). Design of polymethine dyes with large third-order optical nonlinearities and loss figures of merit. *J Science*, *327*(5972), 1485-1488.

Hamberg, I., & Granqvist, C. G. J. J. o. A. P. (1986). Evaporated Sn-doped In2O3 films: Basic optical properties and applications to energy-efficient windows. *60*(11), R123-R160.

Hanson, E., Shen, Y., & Wong, G. (1976). Optical-field-induced refractive indices and orientational relaxation times in a homologous series of isotropic nematic substances. *Physical Review A*, *14*(3), 1281.

He, G., & Liu, S. H. (1999). *Physics of nonlinear optics*. World Scientific.

Heiman, D., Hellwarth, R., Levenson, M., & Martin, G. (1976). Raman-induced Kerr effect. *Physical Review Letters*, *36*(4), 189.

Hellwarth, R., Owyoung, A., & George, N. (1971). Origin of the Nonlinear Refractive Index of Liquid C Cl 4. *Physical Review A*, *4*(6), 2342.

Hendry, E., Hale, P. J., Moger, J., Savchenko, A., & Mikhailov, S. A. (2010). Coherent nonlinear optical response of graphene. *Physical Review Letters*, *105*(9), 097401.

Hercher, M., Chu, W., & Stockman, D. (1968). An experimental study of saturable absorbers for ruby lasers. *IEEE Journal of Quantum Electronics*, *4*(11), 954-968.

Hermann, J. (1992). Self-focusing effects and applications using thin nonlinear media. *International Journal of Nonlinear Optical Physics*, *1*(03), 541-561.

Hönninger, C., Paschotta, R., Morier-Genoud, F., Moser, M., & Keller, U. (1999). Q-switching stability limits of continuous-wave passive mode locking. *JOSA B*, *16*(1), 46-56.

Hosono, H., Ohta, H., Orita, M., Ueda, K., & Hirano, M. (2002). Frontier of transparent conductive oxide thin films. *Vacuum*, *66*(3-4), 419-425.

Huh, M. S., Yang, B. S., Song, J., Heo, J., Won, S.-J., Jeong, J. K., Hwang, C. S., & Kim, H. J. J. J. o. T. E. S. (2008). Improving the morphological and optical properties of sputtered indium tin oxide thin films by adopting ultralow-pressure sputtering. *156*(1), J6.

Humphrey, J. L., & Kuciauskas, D. (2006). Optical susceptibilities of supported indium tin oxide thin films. *Journal of applied physics*, *100*(11), 113123.

Ishibashi, S., Higuchi, Y., Ota, Y., & Nakamura, K. (1990). Low resistivity indium–tin oxide transparent conductive films. II. Effect of sputtering voltage on electrical property of films. *Journal of Vacuum Science & Technology A: Vacuum, Surfaces, and Films*, *8*(3), 1403-1406.

Kaiser, W., & Garrett, C. (1961). Two-photon excitation in Ca F 2: Eu 2+. *Physical review letters*, *7*(6), 229.

Kalanoor, B. S., Gouda, L., Gottesman, R., Tirosh, S., Haltzi, E., Zaban, A., & Tischler, Y. R. J. A. P. (2016). Third-order optical nonlinearities in organometallic methylammonium lead iodide perovskite thin films. *J Acs Photonics*, *3*(3), 361-370.

Katayama, M. (1999). Tft-lcd technology. *Thin Solid Films*, *341*(1-2), 140-147.

Kelley, P. (1965). Self-focusing of optical beams. *Physical Review Letters*, *15*(26), 1005.

Kerr, J. (1875). XL. A new relation between electricity and light: Dielectrified media birefringent. *The London, Edinburgh, and Dublin Philosophical Magazine and Journal of Science*, *50*(332), 337-348.

Khurgin, J. B., Clerici, M., Bruno, V., Caspani, L., DeVault, C., Kim, J., Shaltout, A., Boltasseva, A., Shalaev, V. M., & Ferrera, M. (2020a). Adiabatic frequency shifting in epsilon-near-zero materials: the role of group velocity. *Optica*, *7*(3), 226-231.

Khurgin, J. B., Clerici, M., Bruno, V., Caspani, L., DeVault, C., Kim, J., Shaltout, A., Boltasseva, A., Shalaev, V. M., & Ferrera, M. J. O. (2020b). Adiabatic frequency shifting in epsilon-near-zero materials: the role of group velocity. *7*(3), 226-231.

Kim, G. Y., & Kwak, C. H. (2009). Simple Optical Methods for Measuring Optical Nonlinearities and Rotational Viscosity in Nematic Liquid Crystals. *New Developments in Liquid Crystals*, 111.

Kinsey, N., DeVault, C., Kim, J., Ferrera, M., Shalaev, V., & Boltasseva, A. (2015a). Epsilon-near-zero Al-doped ZnO for ultrafast switching at telecom wavelengths. *Optica*, *2*(7), 616-622.

Kinsey, N., DeVault, C., Kim, J., Ferrera, M., Shalaev, V., & Boltasseva, A. J. O. (2015b). Epsilon-near-zero Al-doped ZnO for ultrafast switching at telecom wavelengths. *2*(7), 616-622.

Kirilyuk, A., Kimel, A. V., & Rasing, T. (2010). Ultrafast optical manipulation of magnetic order. *Reviews of Modern Physics*, *82*(3), 2731.

Kogelnik, H., & Li, T. (1966). Laser beams and resonators. *Applied optics*, *5*(10), 1550-1567.

Köstlin, H., Jost, R., & Lems, W. (1975). Optical and electrical properties of doped In2O3 films. *physica status solidi (a)*, *29*(1), 87-93.

Kowalevicz, A., Sharma, V., Ippen, E., Fujimoto, J. G., & Minoshima, K. J. O. l. (2005). Three-dimensional photonic devices fabricated in glass by use of a femtosecond laser oscillator. *30*(9), 1060-1062.

Kumar, S., Shibu, E., Pradeep, T., & Sood, A. (2013). Ultrafast photoinduced enhancement of nonlinear optical response in 15-atom gold clusters on indium tin oxide conducting film. *Optics Express*, *21*(7), 8483-8492.

Lee, K.-H., Cho, W.-R., Park, J.-H., Kim, J.-S., Park, S.-H., & Kim, U. J. O. l. (1994). Measurement of free-carrier nonlinearities in ZnSe based on the Z-scan technique with a nanosecond laser. *J Optics letters*, *19*(15), 1116-1118.

Li, C. (2017a). Nonlinear Absorption and Refraction of Light. In *Nonlinear Optics* (pp. 177-214). Springer.

Li, C. (2017b). Optical Kerr Effect and Self-focusing. In *Nonlinear Optics* (pp. 109-147). Springer.

Li, C., Wang, R., & Liu, H.-K. (2000). Nonlinear optical limiters with grating sandwich structure for eye protection. *Journal of Nonlinear Optical Physics & Materials*, *9*(04), 413-422.

Li, C., Zhang, L., Wang, R., Song, Y., & Wang, Y. (1994). Dynamics of reverse saturable absorption and all-optical switching in C 60. *JOSA B*, *11*(8), 1356-1360.

Li, C., Zhang, L., Yang, M., Wang, H., & Wang, Y. (1994). Dynamic and steady-state behaviors of reverse saturable absorption in metallophthalocyanine. *Physical Review A*, *49*(2), 1149.

Li, H., Kam, C., Lam, Y., & Ji, W. (2001). Femtosecond Z-scan measurements of nonlinear refraction in nonlinear optical crystals. *Optical materials*, *15*(4), 237-242.

Li, R., Dong, N., Ren, F., Amekura, H., Wang, J., & Chen, F. (2018). Nonlinear absorption response correlated to embedded Ag nanoparticles in BGO single crystal: from two-photon to three-photon absorption. *Scientific Reports*, *8*(1), 1-8.

Li, Y., Liu, J.-L., Chao, T.-S., & Sze, S. (2001). A new parallel adaptive finite volume method for the numerical simulation of semiconductor devices. *Computer physics communications*, *142*(1-3), 285-289.

Li, Y., Yamada, K., Ishizuka, T., Watanabe, W., Itoh, K., & Zhou, Z. J. O. E. (2002). Single femtosecond pulse holography using polymethyl methacrylate. *10*(21), 1173-1178.

Lien, S.-Y. J. T. S. F. (2010). Characterization and optimization of ITO thin films for application in heterojunction silicon solar cells. *518*(21), S10-S13.

Liu, X., Guo, Q., & Qiu, J. J. A. M. (2017). Emerging low-dimensional materials for nonlinear optics and ultrafast photonics. *J Advanced Materials*, *29*(14), 1605886.

Liu, X., & Tomita, Y. (2012). Closed-aperture Z-scan analysis for nonlinear media with saturable absorption and simultaneous third-and fifth-order nonlinear refraction. *Physics Research International*, *2012*.

Liu, Y., Zhou, J., Zhang, X., Liu, Z., Wan, X., Tian, J., Wang, T., & Chen, Y. J. C. (2009). Synthesis, characterization and optical limiting property of covalently oligothiophene-functionalized graphene material. *47*(13), 3113-3121.

Ma, H., Zhao, Y., Shao, Y., Lian, Y., Zhang, W., Hu, G., Leng, Y., & Shao, J. (2021a). Principles to tailor the saturable and reverse saturable absorption of epsilon-near-zero material. *Photonics Research*, *9*(5), 678-686.

Ma, H., Zhao, Y., Shao, Y., Lian, Y., Zhang, W., Hu, G., Leng, Y., & Shao, J. J. P. R. (2021b). Principles to tailor the saturable and reverse saturable absorption of epsilon-near-zero material. *9*(5), 678-686.

Ma, Z., Li, Z., Liu, K., Ye, C., & Sorger, V. J. (2015a). Indium-tin-oxide for high-performance electro-optic modulation. *Nanophotonics*, *4*(2), 198-213.

Ma, Z., Li, Z., Liu, K., Ye, C., & Sorger, V. J. J. N. (2015b). Indium-tin-oxide for high-performance electro-optic modulation. *4*(2), 198-213.

Mançois, F., Pozzo, J. L., Pan, J., Adamietz, F., Rodriguez, V., Ducasse, L., Castet, F., Plaquet, A., & Champagne, B. J. C. A. E. J. (2009). Two-way molecular switches with large nonlinear optical contrast. *15*(11), 2560-2571.

Manoj, P., Joseph, B., Vaidyan, V., & Amma, D. S. D. (2007). Preparation and characterization of indium-doped tin oxide thin films. *Ceramics International*, *33*(2), 273-278.

Maruo, S., Nakamura, O., & Kawata, S. (1997a). Three-dimensional microfabrication with two-photon-absorbed photopolymerization. *Optics letters*, *22*(2), 132-134.

Maruo, S., Nakamura, O., & Kawata, S. J. O. l. (1997b). Three-dimensional microfabrication with two-photon-absorbed photopolymerization. *22*(2), 132-134.

Masters, B. R., & Boyd, R. W. (2009). Book review: nonlinear optics. In: SPIE.

Mattox, D. M., & Mattox, V. H. (2007). 50 Years of Vacuum Coating Technology and the growth of the Society of Vacuum Coaters.

Mcmaster, H. A. (1947). Conductive coating for glass and method of application. In: Google Patents.

Mei, Y., Chen, G., Li, X., Lu, G. Q., & Chen, X. (2013). Evolution of curvature under thermal cycling in sandwich assembly bonded by sintered nanosilver paste. *Soldering & Surface Mount Technology*.

Miguez, M., Barbano, E., Zilio, S. C., & Misoguti, L. J. O. E. (2014). Accurate measurement of nonlinear ellipse rotation using a phase-sensitive method. *J Optics Express*, *22*(21), 25530-25538.

Min, W., Freudiger, C. W., Lu, S., & Xie, X. S. J. A. r. o. p. c. (2011). Coherent nonlinear optical imaging: beyond fluorescence microscopy. *J Annual review of physical chemistry*, *62*, 507.

Minami, T. (2005). Transparent conducting oxide semiconductors for transparent electrodes. *Semiconductor science and technology*, *20*(4), S35.

Mlyuka, N., Niklasson, G. A., & Granqvist, C.-G. (2009). Thermochromic multilayer films of VO2 and TiO2 with enhanced transmittance. *Solar Energy Materials and Solar Cells*, *93*(9), 1685-1687.

Moran, M., She, C.-Y., & Carman, R. J. I. J. o. Q. E. (1975). Interferometric measurements of the nonlinear refractive-index coefficient relative to CS 2 in laser-system-related materials. *J IEEE Journal of Quantum Electronics*, *11*(6), 259-263.

Mukhopadhyay, S., Risko, C., Marder, S. R., & Brédas, J.-L. J. C. S. (2012). Polymethine dyes for all-optical switching applications: a quantum-chemical characterization of counter-ion and aggregation effects on the third-order nonlinear optical response. *J Chemical Science*, *3*(10), 3103-3112.

Nadaud, N., Lequeux, N., Nanot, M., Jove, J., & Roisnel, T. (1998a). Structural studies of tin-doped indium oxide (ITO) and In4Sn3O12. *Journal of Solid State Chemistry*, *135*(1), 140-148.

Nadaud, N., Lequeux, N., Nanot, M., Jove, J., & Roisnel, T. J. J. o. S. S. C. (1998b). Structural studies of tin-doped indium oxide (ITO) and In4Sn3O12. *135*(1), 140-148.

Nagaraja, K., Pramodini, S., Poornesh, P., & Nagaraja, H. (2013). Effect of annealing on the structural and nonlinear optical properties of ZnO thin films under cw regime. *Journal of Physics D: Applied Physics*, *46*(5), 055106.

New, G. (2011). *Introduction to nonlinear optics*. Cambridge University Press.

Owyoung, A. J. I. J. o. Q. E. (1973). Ellipse rotation studies in laser host materials. *J IEEE Journal of Quantum Electronics*, *9*(11), 1064-1069.

Pan, Z. W., Dai, Z. R., & Wang, Z. L. (2001). Nanobelts of semiconducting oxides. *Science*, *291*(5510), 1947-1949.

Park, J.-W., Kim, G., Lee, S.-H., Kim, E.-H., & Lee, G.-H. (2010). The effect of film microstructures on cracking of transparent conductive oxide (TCO) coatings on polymer substrates. *Surface and Coatings Technology*, *205*(3), 915-921.

Park, J.-W., Kim, G., Lee, S.-H., Kim, E.-H., Lee, G.-H. J. S., & Technology, C. (2010). The effect of film microstructures on cracking of transparent conductive oxide (TCO) coatings on polymer substrates. *205*(3), 915-921.

Petkova, P., Vasilev, P., Mustafa, M., Parushev, I., & Soltani, M. (2016). Near-infrared dispersion and spin–orbit interaction of Co doped (80− x) Sb2O3–20Na2O–xWO3 glasses. *Spectrochimica Acta Part A: Molecular and Biomolecular Spectroscopy*, *152*, 475-479.

Philip, R., Kumar, G. R., Sandhyarani, N., & Pradeep, T. (2000). Picosecond optical nonlinearity in monolayer-protected gold, silver, and gold-silver alloy nanoclusters. *Physical Review B*, *62*(19), 13160.

Pokaipisit, A., Horprathum, M., & Limsuwan, P. (2007). Effect of films thickness on the properties of ITO thin films prepared by electron beam evaporation. *Agriculture and Natural Resources*, *41*(5), 255-261.

Pokaipisit, A., Horprathum, M., & Limsuwan, P. (2008). Influence of annealing temperature on the properties of ITO films prepared by electron beam evaporation and ion-assisted deposition. *Agriculture and Natural Resources*, *42*(5), 362-366.

Popov, S. V., Yu, P. S., & Zheludev, N. I. (2017). *Susceptibility tensors for nonlinear optics*. Routledge.

Razeghi, M. (2002). Short-wavelength solar-blind detectors-status, prospects, and markets. *Proceedings of the IEEE*, *90*(6), 1006-1014.

Reyna, A. S., Russier-Antoine, I., Bertorelle, F., Benichou, E., Dugourd, P., Antoine, R., Brevet, P.-F., & de Araújo, C. B. J. T. J. o. P. C. C. (2018). Nonlinear refraction and absorption of Ag29 nanoclusters: evidence for two-photon absorption saturation. *The Journal of Physical Chemistry C*, *122*(32), 18682-18689.

Rumi, M., & Perry, J. W. (2010). Two-photon absorption: an overview of measurements and principles. *Advances in Optics and Photonics*, *2*(4), 451-518.

Said, A., Sheik-Bahae, M., Hagan, D. J., Wei, T., Wang, J., Young, J., & Van Stryland, E. W. (1992). Determination of bound-electronic and free-carrier nonlinearities in ZnSe, GaAs, CdTe, and ZnTe. *JOSA B*, *9*(3), 405-414.

Santos, S., Almeida, J., Paula, K., Tomazio, N., Mastelaro, V. R., & Mendonça, C. R. J. O. M. (2017). Characterization of the third-order optical nonlinearity spectrum of barium borate glasses. *73*, 16-19.

Sauter, E. (1996). *Nonlinear optics* (Vol. 44). John Wiley & Sons.

Shehata, A., & Mohamed, T. J. J. B. (2019). Method for an accurate measurement of nonlinear refractive index in the case of high-repetition-rate femtosecond laser pulses. *JOSA B*, *36*(5), 1246-1251.

Shehata, A., Tawfik, W. Z., & Mohamed, T. J. J. B. (2020). Cobalt enhanced nonlinear optical properties and optical limiting of zinc oxide irradiated by femtosecond laser pulses. *JOSA B*, *37*(11), A1-A8.

Sheik-Bahae, M., & Hasselbeck, M. P. (2000). Third-order optical nonlinearities. *Handbook of Optics*, *4*, 16.11-16.36.

Sheik-Bahae, M., Said, A. A., Hagan, D. J., Soileau, M., & Van Stryland, E. W. (1991). Nonlinear refraction and optical limiting in. *Optical engineering*, *30*(8), 1228-1235.

Sheik-Bahae, M., Said, A. A., & Van Stryland, E. W. (1989a). High-sensitivity, single-beam n 2 measurements. *Optics letters*, *14*(17), 955-957.

Sheik-Bahae, M., Said, A. A., & Van Stryland, E. W. J. O. l. (1989b). High-sensitivity, single-beam n 2 measurements. *J Optics letters*, *14*(17), 955-957.

Sheik-Bahae, M., Said, A. A., Wei, T.-H., Hagan, D. J., & Van Stryland, E. W. (1990). Sensitive measurement of optical nonlinearities using a single beam. *IEEE journal of quantum electronics*, *26*(4), 760-769.

Shen, Y.-R. (1984). Principles of nonlinear optics.

Shen, Y. (1966). Electrostriction, optical Kerr effect and self-focusing of laser beams. *Physics Letters*, *20*(4), 378-380.

So, P., Dong, C., Masters, B., & Berland, K. (2000). Two-photon excitation fluorescence microscopy.

Soileau, M., Williams, W. E., Van Stryland, E. W., Boggess, T. F., & Smirl, A. L. J. O. E. (1983). Picosecond damage studies at 0.5 and 1 μm. *J Optical Engineering*, *22*(4), 424-430.

Song, Y., Fang, G., Wang, Y., Liu, S., Li, C., Song, L., Zhu, Y., & Hu, Q. (1999). Excited-state absorption and optical-limiting properties of organometallic fullerene–C 60 derivatives. *Applied physics letters*, *74*(3), 332-334.

Sridharan, K., Sreekanth, P., Park, T. J., & Philip, R. J. T. J. o. P. C. C. (2015). Nonlinear optical investigations in nine-atom silver quantum clusters and graphitic carbon nitride nanosheets. *119*(28), 16314-16320.

Stadler, A. (2012). Transparent conducting oxides—an up-to-date overview. *Materials*, *5*(4), 661-683.

Strickler, J. H., & Webb, W. W. (1991). Three-dimensional optical data storage in refractive media by two-photon point excitation. *Optics letters*, *16*(22), 1780-1782.

Strickler, J. H., & Webb, W. W. J. O. l. (1991). Three-dimensional optical data storage in refractive media by two-photon point excitation. *16*(22), 1780-1782.

Stucky, G. D., Phillips, M. L., & Gier, T. E. (1989). The potassium titanyl phosphate structure field: a model for new nonlinear optical materials. *Chemistry of materials*, *1*(5), 492-509.

Szöke, A., & Javan, A. (1963). Isotope shift and saturation behavior of the 1.15− μ transition of Ne. *Physical Review Letters*, *10*(12), 521.

Tian, X., Wei, R., Guo, Q., Zhao, Y. J., & Qiu, J. J. A. M. (2018). Reverse Saturable Absorption Induced by Phonon-Assisted Anti-Stokes Processes. *J Advanced Materials*, *30*(28), 1801638.

Tutt, L. W., & Boggess, T. F. J. P. i. q. e. (1993). A review of optical limiting mechanisms and devices using organics, fullerenes, semiconductors and other materials. *Progress in quantum electronics*, *17*(4), 299-338.

Ule, E. (2015). Measurement of the nonlinear refractive index by Z-scan technique. *University of Ljubljana, Slovenia*, 4-5.

Van Stryland, E. W., & Hagan, D. J. (2003). Nonlinear absorption. *Encyclopedia of optical engineering*, 1475-1481.

Van Stryland, E. W., Wu, Y.-Y., Hagan, D. J., Soileau, M., & Mansour, K. (1988a). Optical limiting with semiconductors. *JOSA B*, *5*(9), 1980-1988.

Van Stryland, E. W., Wu, Y.-Y., Hagan, D. J., Soileau, M., & Mansour, K. J. J. B. (1988b). Optical limiting with semiconductors. *5*(9), 1980-1988.

Vasconcelos, H. C. (2022). Optical Nonlinearities in Glasses. In *Nonlinear Optics-Nonlinear Nanophotonics and Novel Materials for Nonlinear Optics*. IntechOpen.

Wager, J. F. J. s. (2003). Transparent electronics. *300*(5623), 1245-1246.

Walden, S. L. (2017). *Nonlinear optical properties of ZnO and ZnO-Au composite nanostructures for nanoscale UV emission* Queensland University of Technology].

Wang, H., Jiao, X., Liu, Q., Xuan, X., Chen, F., & Wu, W. J. J. o. P. D. A. P. (2010). Transparent and conductive oxide films of the perovskite LaxSr1−xSnO3 (x⩽ 0.15): epitaxial growth and application for transparent heterostructures. *43*(3), 035403.

Wang, W., Liu, Y., Xi, P., & Ren, Q. (2010). Origin and effect of high-order dispersion in ultrashort pulse multiphoton microscopy in the 10 fs regime. *Applied optics*, *49*(35), 6703-6709.

Weaire, D., Wherrett, B., Miller, D., & Smith, S. (1979). Effect of low-power nonlinear refraction on laser-beam propagation in InSb. *Optics Letters*, *4*(10), 331-333.

Weiner, A. M. J. O. C. (2011). Ultrafast optical pulse shaping: A tutorial review. *284*(15), 3669-3692.

White, M. A. (2018). *Physical properties of materials*. CRC press.

Williams, W. E., Soileau, M., & Van Stryland, E. W. J. O. c. (1984). Optical switching and n2 measurements in CS2. *J Optics communications*, *50*(4), 256-260.

Wohlmuth, W., & Adesida, I. J. T. S. F. (2005). Properties of RF magnetron sputtered cadmium–tin–oxide and indium–tin–oxide thin films. *479*(1-2), 223-231.

Wong, G. K., & Shen, Y. (1974). Study of pretransitional behavior of laser-field-induced molecular alignment in isotropic nematic substances. *Physical Review A*, *10*(4), 1277.

Xiao, Q.-H., Feng, X.-Y., Yang, W., Lin, Y.-K., Peng, Q.-Q., Jiang, S.-Z., Liu, J., & Su, L.-B. (2020a). Epsilon-near-zero indium tin oxide nanocolumns

array as a saturable absorber for a Nd: BGO laser. *Laser Physics*, *30*(5), 055802.

Xiao, Q.-H., Feng, X.-Y., Yang, W., Lin, Y.-K., Peng, Q.-Q., Jiang, S.-Z., Liu, J., & Su, L.-B. J. L. P. (2020b). Epsilon-near-zero indium tin oxide nanocolumns array as a saturable absorber for a Nd: BGO laser. *30*(5), 055802.

Yan, T., Hong, R., Tao, C., Wang, Q., Lin, H., Han, Z., & Zhang, D. (2022). Thickness dependency of PVA on the transition from saturable absorption to reverse saturable absorption of ITO films. *Optical Materials*, *125*, 112061.

Zaid, M., Matori, K., Quah, H., Lim, W., Sidek, H., Halimah, M., Yunus, W., & Wahab, Z. J. J. o. M. S. M. i. E. (2015). Investigation on structural and optical properties of SLS–ZnO glasses prepared using a conventional melt quenching technique. *26*(6), 3722-3729.

Zhang, Z., Liu, J., Hao, Q., & Liu, J. (2019). Sensitive saturable absorber and optical switch of epsilon-near-zero medium. *Applied Physics Express*, *12*(6), 065504.

Zheng, X., Zhang, Y., Chen, R., Xu, Z., & Jiang, T. (2015). Z-scan measurement of the nonlinear refractive index of monolayer WS 2. *Optics express*, *23*(12), 15616-15623.